

# Polarized light propagation and scattering in random media

Arnold D. Kim<sup>a</sup>, Sermsak Jaruwatanadilok<sup>b</sup>, Akira Ishimaru<sup>b</sup>, and Yasuo Kuga<sup>b</sup>

<sup>a</sup>Department of Mathematics, Stanford University, Stanford, CA 94305, USA

<sup>b</sup>Department of Electrical Engineering, University of Washington, Seattle, WA 98195, USA

## ABSTRACT

Using radiative transfer, we investigate linear and circular polarized light normally impinging a plane-parallel medium containing a random distribution of identically sized latex spheres in water. The focus of this study is to understand fundamental properties of polarized light scattering. In particular, we analyze backscattered and transmitted flux responses computed from direct numerical simulations. From these numerical computations, we observe that circular polarized light depolarizes at a slower rate than linear polarized light. In addition, circular polarized light shows a more noticeable dependence on the size of the scatterers than linear polarized light. Furthermore, the helicity flip observed in circular polarized backscattered light is a fundamental phenomenon manifested by low order scattering.

**Keywords:** Radiative transfer, Stokes parameters, polarization, Mie scattering

## 1. INTRODUCTION

To describe the effects of scattering on the polarization state of electromagnetic waves, the theory of radiative transfer generalizes to model the evolution of the Stokes vector of the specific intensity.<sup>1,2</sup> Because the inclusion of polarization presents significantly more complex mathematics, less theoretical work has been done on these problems. Recently, however, there has been a number of experimental and theoretical studies regarding polarized light propagation and scattering in random media for applications in tissue imaging.<sup>3-7</sup> Various experiments have demonstrated that depolarization requires longer length scales than those needed for diffusion. In that case, polarization characteristics of scattered waves provide another, and potentially more effective, way to discriminate between different kinds of optically thick media.

Since changes in polarization only occur from scattering, early transmitted responses co-polarized with the incident light have suffered very little scattering. Therefore, examining the polarization state of transmitted responses by scattering media provides a simple and effective way to discriminate between ballistic and snake photons from diffuse ones in optically thick media. This intuition has led to a number of imaging and detection methods and techniques.<sup>4-8</sup> Many have also examined differences between linear and circular polarized incident light.<sup>9-12</sup> Except for very small scatterers, experimental evidence clearly suggests that circular polarized light transmitted through a scattering medium made up of spherical scatterers requires significantly more scattering to depolarize than linear polarized light. While this phenomenon is present in a variety of settings, this difference is most pronounced for spherical scatterers that are much larger than the wavelength of the incident light.<sup>9,13,14</sup> In contrast, experiments show that linear polarized light depolarizes more slowly than circular polarized light for actual tissue samples.<sup>11,12</sup>

Backscattered responses by polarized light also exhibit interesting phenomena. Backscattered circular polarized light maintains a significant degree of polarization.<sup>15</sup> In addition, backscattered circular polarized light exhibits a helicity flip.<sup>15</sup> In other words, the helicity channel from which you would expect more backscattering (i.e. the channel in which you would receive specular reflection from a perfectly conducting plate) in fact has less than the other helicity channel. The extent of these phenomena strongly depends on the sphere size. There has been some theoretical efforts to examine and predict the mechanisms of these phenomena,<sup>15,16</sup> although these efforts are not entirely exhaustive. Regardless, properties of circularly polarized backscattered light allow for an effective strategy to detect targets in scattering media.<sup>17</sup>

In this paper, we investigate the fundamental characteristics of polarized wave scattering in random media. Since there seems to be a broad variety of complicated phenomena present in these problems, our objective is to solve

---

Further author information: (Send correspondence to Arnold D. Kim)

Department of Mathematics; 450 Serra Mall Building 380; Stanford University; Stanford, CA 94305-2125; Phone: (650) 723-1917, Fax: (650) 725-4066, E-mail: adkim@math.stanford.edu

a problem from which we ascertain an understanding of the very basic polarization characteristics in scattering media. To fulfill this objective, we solve the vector radiative transfer equation for a plane-parallel medium due to polarized (linear and circular) incident plane waves using direct numerical simulations. This plane-parallel medium has index-matched boundaries and contains a random distribution of identically sized latex spheres. We use Mie theory to compute the exact representation of the scattering operations. Although we are considering an ideal case where boundaries are index-matched and scatterers are identically sized spheres, we are most interested in examining fundamental multiple scattering effects on polarized waves. Therefore, we examine this simple setting to evaluate polarization without simplifying the scattering description.

We begin by reviewing the radiative transfer equations for plane-parallel problems with linearly and circularly polarized incident plane waves. Next, we present results from direct numerical computations of these vector radiative transfer equations. We compute these solutions using the Chebyshev Spectral Method.<sup>18</sup> From this data, we analyze transmitted and backscattered flux responses and the differences between linear and circular polarization. Finally, we conclude with a summary of our results regarding multiple scattering effects on polarized light.

## 2. VECTOR RADIATIVE TRANSFER

Consider a polarized plane wave normally impinging a plane-parallel medium containing a random distribution of identically sized spheres. The vector radiative transfer equation governing the diffuse modified Stokes vector  $\bar{\mathbf{I}}$  for this problem<sup>19,20</sup> is

$$\mu \frac{\partial}{\partial \tau} \bar{\mathbf{I}}(\tau, \mu, \phi) + \bar{\mathbf{I}}(\tau, \mu, \phi) = \int_0^{2\pi} \int_{-1}^1 S(\mu, \phi, \mu', \phi') \bar{\mathbf{I}}(\tau, \mu', \phi') d\mu' d\phi' + \bar{\mathbf{f}}(\tau, \mu, \phi), \quad (1)$$

over the domain,  $0 \leq \tau < \tau_o$ . Here  $\mu = \cos \theta$ ,  $\tau = \rho \sigma_t z$ , and  $\tau_o = \rho \sigma_t d$  where  $\rho$  is the number density of scatterers and  $\sigma_t$  is the total scattering cross-section. Since we assume that all of the spherical scatterers have identical radii,  $\sigma_t$  is a constant. Furthermore, we assume that this incident wave provides the only source of radiation in the medium whose boundaries are index-matched so that

$$\bar{\mathbf{I}}(\tau = 0, \mu, \phi) = 0 \quad \text{for } 0 < \mu \leq 1 \quad (2a)$$

$$\bar{\mathbf{I}}(\tau = \tau_o, \mu, \phi) = 0 \quad \text{for } -1 \leq \mu < 0. \quad (2b)$$

The kernel of the integral operator in (1) is the Mueller matrix which gives the scattered Stokes vector observed in the  $(\mu, \phi)$  direction by an incident Stokes vector in the  $(\mu', \phi')$  direction from an individual scatterer.<sup>2,21</sup> The Mueller matrix is

$$S(\mu, \phi, \mu', \phi') = \sigma_t^{-1} \begin{bmatrix} |f_{11}|^2 & |f_{12}|^2 & \text{Re}(f_{11}f_{12}^*) & -\text{Im}(f_{11}f_{12}^*) \\ |f_{21}|^2 & |f_{22}|^2 & \text{Re}(f_{21}f_{22}^*) & -\text{Im}(f_{21}f_{22}^*) \\ 2\text{Re}(f_{11}f_{21}^*) & 2\text{Re}(f_{12}f_{22}^*) & \text{Re}(f_{11}f_{22}^* + f_{12}f_{21}^*) & -\text{Im}(f_{11}f_{22}^* - f_{12}f_{21}^*) \\ 2\text{Im}(f_{11}f_{21}^*) & 2\text{Im}(f_{12}f_{22}^*) & \text{Im}(f_{11}f_{22}^* + f_{12}f_{21}^*) & \text{Re}(f_{11}f_{22}^* - f_{12}f_{21}^*) \end{bmatrix} \quad (3)$$

where  $\{f_{11}, f_{12}, f_{21}, f_{22}\}$  is the set of scattering amplitudes.<sup>2</sup> Throughout this paper, we refer to the submatrices of the Mueller matrix,  $\{S_1, S_2, S_3, S_4\}$ , where

$$S = \begin{bmatrix} S_1 & S_2 \\ S_3 & S_4 \end{bmatrix}. \quad (4)$$

For spherical scatterers, Mie theory provides the exact expressions for these scattering amplitudes.<sup>2,21-24</sup> The results of Mie theory are summarized by two complex amplitude functions:<sup>23</sup>  $s_1$  and  $s_2$ , from which one is able to compute these scattering amplitudes and hence, the Mueller matrix.<sup>20</sup>

The source term  $\bar{\mathbf{f}}(\tau, \mu, \phi)$  in (1) is the contribution from the reduced intensity corresponding to the incident plane wave. We consider two cases below: linearly and circularly polarized incident plane waves. R. L.-T. Cheung and A. Ishimaru give a full derivation for both cases,<sup>20</sup> so we only summarize the main results here.

## 2.1. Linearly Polarized Incident Plane Wave

To treat the azimuthal dependence in (1), let us consider a Fourier expansion of the Stokes vector

$$\bar{\mathbf{I}}(\tau, \mu, \phi) = \bar{\mathbf{I}}^{(0)}(\tau, \mu) + \sum_{n=1}^{\infty} \left[ \bar{\mathbf{I}}_c^{(n)}(\tau, \mu) \cos(n\phi) + \bar{\mathbf{I}}_s^{(n)}(\tau, \mu) \sin(n\phi) \right]. \quad (5)$$

For normally incident, linearly polarized plane waves, we find that the mode zero and mode two Fourier modes of this series are the only ones that are non-zero.<sup>20</sup> This simplification is a manifestation of the azimuthal symmetry of the Mueller matrix constructed from Mie theory.

The equation for the Fourier mode zero term is

$$\mu \frac{\partial}{\partial \tau} \bar{\Psi}_0(\tau, \mu) + \bar{\Psi}_0(\tau, \mu) = \int_{-1}^1 \mathbf{L}^{(0)}(\mu, \mu') \bar{\Psi}_0(\tau, \mu') d\mu' + \bar{\mathbf{F}}^{(0)}(\mu) \exp[-\tau], \quad (6)$$

where

$$\bar{\Psi}_0(\tau, \mu) = \begin{bmatrix} I_1^{(0)}(\tau, \mu) \\ I_2^{(0)}(\tau, \mu) \end{bmatrix}, \quad (7)$$

and

$$\bar{\mathbf{F}}^{(0)}(\mu) = \frac{1}{2\sigma_t} \begin{bmatrix} |A_{ll}(\mu)|^2 \\ |A_{rr}(\mu)|^2 \end{bmatrix}. \quad (8)$$

The functions,  $A_{ll}$  and  $A_{rr}$  are proportional to the complex scattering amplitudes,<sup>20</sup>

$$A_{ll} = is_2^*/k, \quad \text{and} \quad A_{rr} = is_1^*/k. \quad (9)$$

The kernel of the scattering operator,  $\mathbf{L}_1^{(0)}(\mu, \mu')$ , is mode zero term of the Fourier series expansion of the  $S_1$  submatrix,

$$\mathbf{L}_1^{(0)}(\mu, \mu') = \int_0^{2\pi} S_1(\mu, \mu', \phi' - \phi) d(\phi' - \phi). \quad (10)$$

The vector,  $\bar{\Psi}_0$ , satisfies

$$\bar{\Psi}_0(\tau = 0, \mu) = 0 \quad \text{for } 0 < \mu \leq 1 \quad (11a)$$

$$\bar{\Psi}_0(\tau = \tau_o, \mu) = 0 \quad \text{for } -1 \leq \mu < 0. \quad (11b)$$

The equation for the Fourier mode two term is

$$\mu \frac{\partial}{\partial \tau} \bar{\Psi}_2(\tau, \mu) + \bar{\Psi}_2(\tau, \mu) = \int_{-1}^1 \mathbf{L}^{(2)}(\mu, \mu') \bar{\Psi}_2(\tau, \mu') d\mu' + \bar{\mathbf{F}}^{(2)}(\mu) \exp[-\tau], \quad (12)$$

where

$$\bar{\Psi}_2(\tau, \mu) = \begin{bmatrix} I_{1c}^{(2)}(\tau, \mu) \\ I_{2c}^{(2)}(\tau, \mu) \\ U_s^{(2)}(\tau, \mu) \\ V_s^{(2)}(\tau, \mu) \end{bmatrix} \quad (13)$$

and

$$\bar{\mathbf{F}}^{(2)}(\mu) = \frac{1}{2\sigma_t} \begin{bmatrix} |A_{ll}(\mu)|^2 \\ -|A_{rr}(\mu)|^2 \\ -2\text{Re}(A_{ll}(\mu)A_{rr}^*(\mu)) \\ -2\text{Im}(A_{ll}(\mu)A_{rr}^*(\mu)) \end{bmatrix}. \quad (14)$$

The kernel of the scattering operator is made up of four submatrices,

$$\mathbf{L}^{(2)} = \begin{bmatrix} \mathbf{L}_1^{(2)} & \mathbf{L}_2^{(2)} \\ -\mathbf{L}_3^{(2)} & \mathbf{L}_4^{(2)} \end{bmatrix}, \quad (15)$$

where

$$L_1^{(2)}(\mu, \mu') = \int_0^{2\pi} S_1(\mu, \mu', \phi' - \phi) \cos[2(\phi - \phi')] d(\phi' - \phi), \quad (16a)$$

$$L_2^{(2)}(\mu, \mu') = \int_0^{2\pi} S_2(\mu, \mu', \phi' - \phi) \sin[2(\phi - \phi')] d(\phi' - \phi), \quad (16b)$$

$$L_3^{(2)}(\mu, \mu') = \int_0^{2\pi} S_3(\mu, \mu', \phi' - \phi) \sin[2(\phi - \phi')] d(\phi' - \phi), \quad (16c)$$

$$L_4^{(2)}(\mu, \mu') = \int_0^{2\pi} S_4(\mu, \mu', \phi' - \phi) \cos[2(\phi - \phi')] d(\phi' - \phi). \quad (16d)$$

The vector,  $\bar{\Psi}_2$ , satisfies

$$\bar{\Psi}_2(\tau = 0, \mu) = 0 \quad \text{for } 0 < \mu \leq 1 \quad (17a)$$

$$\bar{\Psi}_2(\tau = \tau_o, \mu) = 0 \quad \text{for } -1 \leq \mu < 0. \quad (17b)$$

After solving the mode zero and mode two boundary value problems, we construct the Stokes vector for the diffuse intensity,

$$\bar{\mathbf{I}}(\tau, \mu, \phi) = \begin{bmatrix} I_1 \\ I_2 \\ U \\ V \end{bmatrix} = \begin{bmatrix} I_1^{(0)}(\tau, \mu) \\ I_2^{(0)}(\tau, \mu) \\ 0 \\ 0 \end{bmatrix} + \begin{bmatrix} I_{1c}^{(2)}(\tau, \mu) \cos(2\phi) \\ I_{2c}^{(2)}(\tau, \mu) \cos(2\phi) \\ U_s^{(2)}(\tau, \mu) \sin(2\phi) \\ V_s^{(2)}(\tau, \mu) \sin(2\phi) \end{bmatrix}. \quad (18)$$

To calculate the Stokes vector corresponding to the polarization parallel and perpendicular to the polarization of the incident wave, we apply a rotation on (18),

$$\begin{bmatrix} I_x \\ I_y \\ U_{xy} \\ V_{xy} \end{bmatrix} = \begin{bmatrix} \mu^2 \cos^2 \phi & \sin^2 \phi & -1/2 \mu \sin 2\phi & 0 \\ \mu^2 \sin^2 \phi & \cos^2 \phi & 1/2 \mu \sin 2\phi & 0 \\ \mu^2 \sin 2\phi & -\sin 2\phi & \mu \cos 2\phi & 0 \\ 0 & 0 & 0 & \mu \end{bmatrix} \begin{bmatrix} I_1 \\ I_2 \\ U \\ V \end{bmatrix}, \quad (19)$$

where  $I_x$  is the intensity component polarized parallel to the incident polarization, or co-polarized intensity, and  $I_y$  is the intensity component polarized perpendicular to the incident polarization or cross-polarized intensity.

## 2.2. Circularly Polarized Incident Plane Wave

Let us consider a left-handed circularly polarized incident plane wave. By performing the same Fourier series analysis that we used for the linearly polarized incident wave, we find that only the mode zero Fourier mode is non-zero. Furthermore, we find that (1) reduces to two decoupled equations,

$$\mu \frac{\partial}{\partial \tau} \bar{\Psi}_0(\tau, \mu) + \bar{\Psi}_0(\tau, \mu) = \int_{-1}^1 L_1^{(0)}(\mu, \mu') \bar{\Psi}_0(\tau, \mu') d\mu' + \bar{\mathbf{F}}^{(0)}(\mu) \exp[-\tau], \quad (20)$$

and

$$\mu \frac{\partial}{\partial \tau} \bar{\Phi}_0(\tau, \mu) + \bar{\Phi}_0(\tau, \mu) = \int_{-1}^1 L_4^{(0)}(\mu, \mu') \bar{\Phi}_0(\tau, \mu') d\mu' + \bar{\mathbf{G}}^{(0)}(\mu) \exp[-\tau]. \quad (21)$$

Here (20) is identical to the mode zero equation for the linearly polarized incident wave. In (21), we define

$$\bar{\Phi}_0(\tau, \mu) = \begin{bmatrix} U^{(0)}(\tau, \mu) \\ V^{(0)}(\tau, \mu) \end{bmatrix}, \quad (22)$$

$$\bar{\mathbf{G}}^{(0)}(\mu) = \frac{1}{\sigma_t} \begin{bmatrix} -\text{Im}(A_{ll}(\mu)A_{rr}^*(\mu)) \\ \text{Re}(A_{ll}(\mu)A_{rr}^*(\mu)) \end{bmatrix}, \quad (23)$$

and

$$L_4^{(0)}(\mu, \mu') = \int_0^{2\pi} S_4(\mu, \mu', \phi' - \phi) d(\phi' - \phi). \quad (24)$$

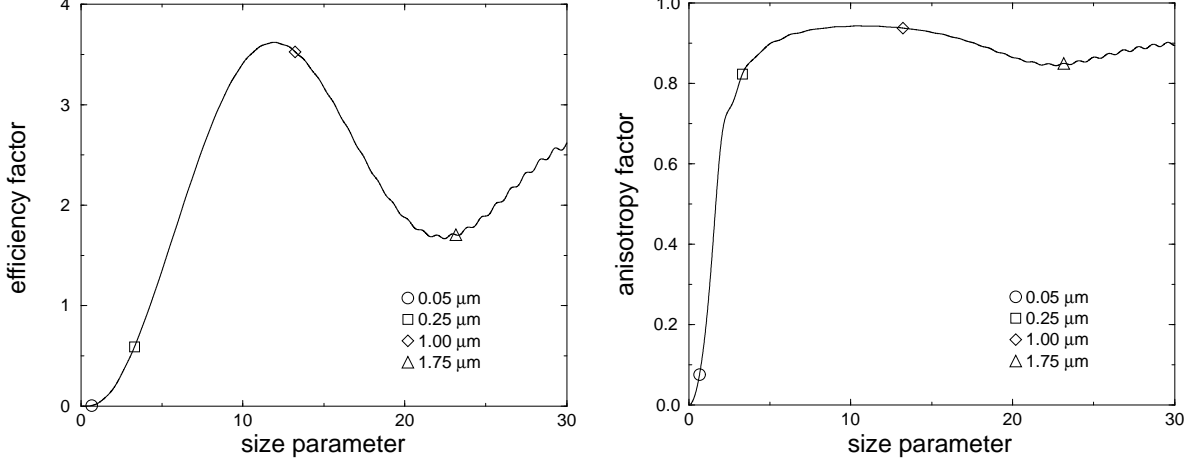


**Figure 1.** The efficiency factor,  $Q_{ext}$ , (left plot) and anisotropy factor,  $\bar{\mu}$ , (right plot) as a function of the size parameter,  $ka$ , for the polystyrene spheres used in the computational simulations calculated using the Mie scattering solution.

The vector,  $\bar{\Phi}_0$ , satisfies

$$\bar{\Phi}_0(\tau = 0, \mu) = 0 \quad \text{for } 0 < \mu \leq 1 \quad (25a)$$

$$\bar{\Phi}_0(\tau = \tau_o, \mu) = 0 \quad \text{for } -1 \leq \mu < 0. \quad (25b)$$

After solving (20) and (21), we determine the left-handed and right-handed circularly polarized intensities,<sup>20</sup>

$$I_{\text{lhc}} = (I_1 + I_2 + V)/2 \quad (26a)$$

$$I_{\text{rhc}} = (I_1 + I_2 - V)/2 \quad (26b)$$

Since we chose the incident wave to be left-handed circularly polarized, we define the transmitted co-polarized and cross-polarized intensities to be

$$I_{\text{co-pol}}^{(\text{trans})} = I_{\text{lhc}}^{(\text{trans})}, \quad \text{and} \quad I_{\text{x-pol}}^{(\text{trans})} = I_{\text{rhc}}^{(\text{trans})}.$$

Furthermore, since (26a) and (26b) are defined with respect to the direction of propagation, the backscattered co-polarized and cross-polarized intensities are

$$I_{\text{co-pol}}^{(\text{back})} = I_{\text{rhc}}^{(\text{back})}, \quad \text{and} \quad I_{\text{x-pol}}^{(\text{back})} = I_{\text{lhc}}^{(\text{back})}.$$

We choose to define the co-polarized backscattered intensity to correspond to the polarization state of a wave specularly reflected by a perfectly conducting plate. Recall that the incident plane wave that we consider is left-handed circularly polarized.

### 3. NUMERICAL RESULTS

We solved the vector radiative transfer equations for linearly and circularly polarized incident plane waves using the Chebyshev Spectral Method.<sup>18</sup> We chose this method because it yields stable and accurate solutions over a large range of optical depths, even for large anisotropy factors. The basis of this method is a Chebyshev spectral approximation of the spatial part of the intensity which results in a coupled system of integral equations. For all of these examples, we used 129 Chebyshev modes, and solved the system of integral equation using a Nyström method employing a 60-point Gaussian quadrature rule that used Legendre polynomial abscissa and weights.

After computing the transmitted and backscattered intensities, we computed the co-polarized and cross-polarized flux magnitudes,

$$\mathbf{F}_{\text{co-pol}} = \int_0^{2\pi} \int_{-1}^1 I_{\text{co-pol}}(\mu, \phi) \mu d\mu d\phi \quad (27a)$$

$$\mathbf{F}_{\text{x-pol}} = \int_0^{2\pi} \int_{-1}^1 I_{\text{x-pol}}(\mu, \phi) \mu d\mu d\phi, \quad (27b)$$

where  $I_{\text{co-pol}}$  and  $I_{\text{x-pol}}$  were evaluated at  $\tau = 0$  for backscattering and  $\tau = \tau_o$  for transmission. The azimuthal angle integrals were analytically calculated since the  $\phi$ -dependence is simple due to the Fourier series expansion. The polar angle integrals were computed using the same Gaussian quadrature rule used to solve the integral equations.

For these numerical simulations, we considered latex spheres randomly distributed in water illuminated by an optical wave generated by a He-Ne laser. The wavelength of light from the He-Ne laser in air is  $\lambda = 632.8$  nm. When light from this laser propagates in water whose refractive index is  $n_{\text{water}} = 1.33$ , its wave number is  $k \approx 13.21 \mu\text{m}^{-1}$ . The refractive index for these latex spheres in this problem is  $n_{\text{spheres}} = 1.588$  so that the relative refractive index of these spheres in water is  $n_{\text{relative}} = 1.19$ .

In particular, we considered four different sphere radii:  $a = 0.05, 0.25, 1.00, \text{ and } 1.75 \mu\text{m}$ . Using the algorithm by Bohren and Huffman,<sup>24</sup> we calculated the efficiency and anisotropy factors for these spheres. A plot of these results appear in Fig. 1 and their size parameters, efficiency factors, and anisotropy factors appear in Table 1. We chose these four sphere sizes to sample the areas near and far from the Mie resonance regime.<sup>22-24</sup> Notice that there is no imaginary part in this relative refractive index so no absorption is present in the medium. Hence, a conservation of power calculation indicates the accuracy of our computations. For these computations, the conservation of power yielded maximum errors of  $\sim 10^{-8}\%$  for the three smallest spheres and  $\sim 10^{-4}\%$  for the largest sphere.

### 3.1. Transmission

In Fig. 2, we plot the transmitted flux responses as a function of optical depth for the four different scatterer sizes (rows) and for linear (left column) and circular (right column) incident polarization.

Since the  $0.05 \mu\text{m}$  radius spheres are much smaller than the wavelength, we expect them to act like Rayleigh scatterers. Therefore, we expect transmitted responses to depolarize for these spheres much more quickly than responses from larger spheres. Our computations agree with this intuition. For both linear and circular incident polarizations, we find that waves depolarize and the difference between the co-polarized and cross-polarized fluxes are negligible for  $\tau_o > 7$ . Although the circular case decays slightly slower than the linear case, this difference is not significant.

For the larger spheres, we see that the transmitted flux responses do not fully depolarize at  $\tau_o = 20$ . Furthermore, we observe that the circularly polarized incident waves maintain a greater difference between its co-polarized and cross-polarized fluxes than linearly polarized incident waves. In Table 2, we summarize the differences between the co-polarized and cross-polarized fluxes. We observe that the largest flux differences occur for the near-resonant scatterers whose radii are  $1.00 \mu\text{m}$ . For that case, we observe that responses from linearly polarized waves exhibit a 2 dB difference while those from circularly polarized waves exhibit a 7 dB difference. For the non-resonant scatterers, we observe that the flux differences are small for linear polarized incident waves compared with those for circularly polarized ones. However, all of these flux differences exhibit a strong dependence on the sphere radius. Most

**Table 1.** Size parameters, efficiency factors, and anisotropy factors of the four different sphere radii used in our computations.

radius ( $\mu\text{m}$ )	$ka$	$Q_{ext}$	$\bar{\mu}$
0.05	0.66	0.00558	0.0752
0.25	3.31	0.590	0.823
1.00	13.23	3.526	0.938
1.75	22.15	1.705	0.850

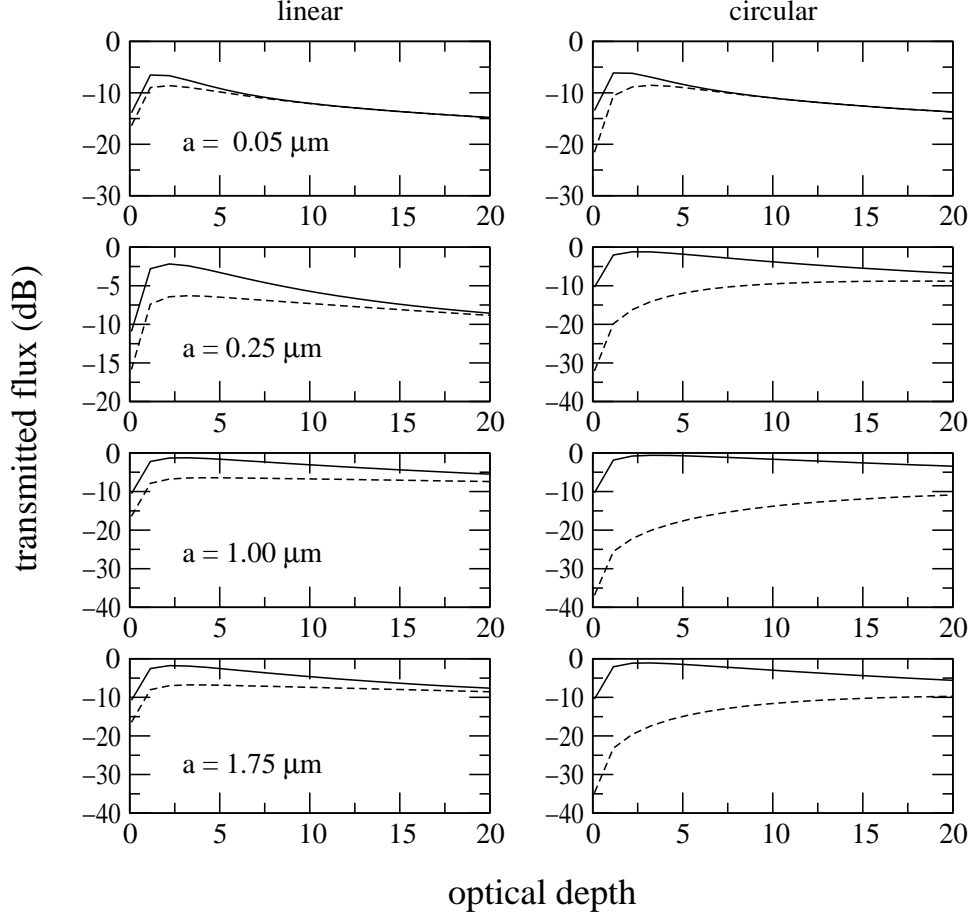


**Figure 2.** The diffuse transmitted flux responses for the linearly polarized waves (left column) and circularly polarized waves (right column). The plots on the first row from the top correspond to  $0.05\mu\text{m}$  radius spheres; the second row corresponds to  $0.25\mu\text{m}$  radius spheres; the third row corresponds to  $1.00\mu\text{m}$  radius spheres; and the fourth row corresponds to  $1.75\mu\text{m}$  radius spheres. The solid lines correspond to the co-polarized flux and the dashed lines correspond to the cross-polarized flux.

likely, this dependence is due to the large anisotropy factors of these scatterers. Transmitted flux quantities are weighted more heavily in forward directions. In addition, scattering in forward directions maintains a large degree of polarization compared with other directions. Hence, highly anisotropy scattering in which the angular spectrum is strongly peaked in the forward direction also exhibits a sizable degree of polarization.

### 3.2. Backscattering

In Fig. 3, we plot the backscattered flux responses as a function of optical depth for the four different scatterer sizes (rows) and for linear (left column) and circular (right column) incident polarization.

For  $0.05\mu\text{m}$  radius spheres, we observe that the backscattered flux responses exhibit  $\sim 1.5$  dB differences between the co-polarized and cross-polarized flux for both linear and circular cases. The differences between the linear and circular cases are small and qualitatively similar. These fluxes saturate to a constant as the optical depth approaches infinity. For larger spheres, we observe that the flux responses due to linearly polarized incident waves are all qualitatively similar. While these flux responses do not completely depolarize, the differences between the co-polarized and cross-polarized flux are small. From Table 2, we observe that flux differences at  $\tau_o = 20$  occur within fractions of a dB. This behavior persists for optical depths  $\tau_o > 7$ . Therefore, the backscattered flux responses by linearly polarized incident waves do not exhibit a strong dependence on different scatterer sizes. In contrast

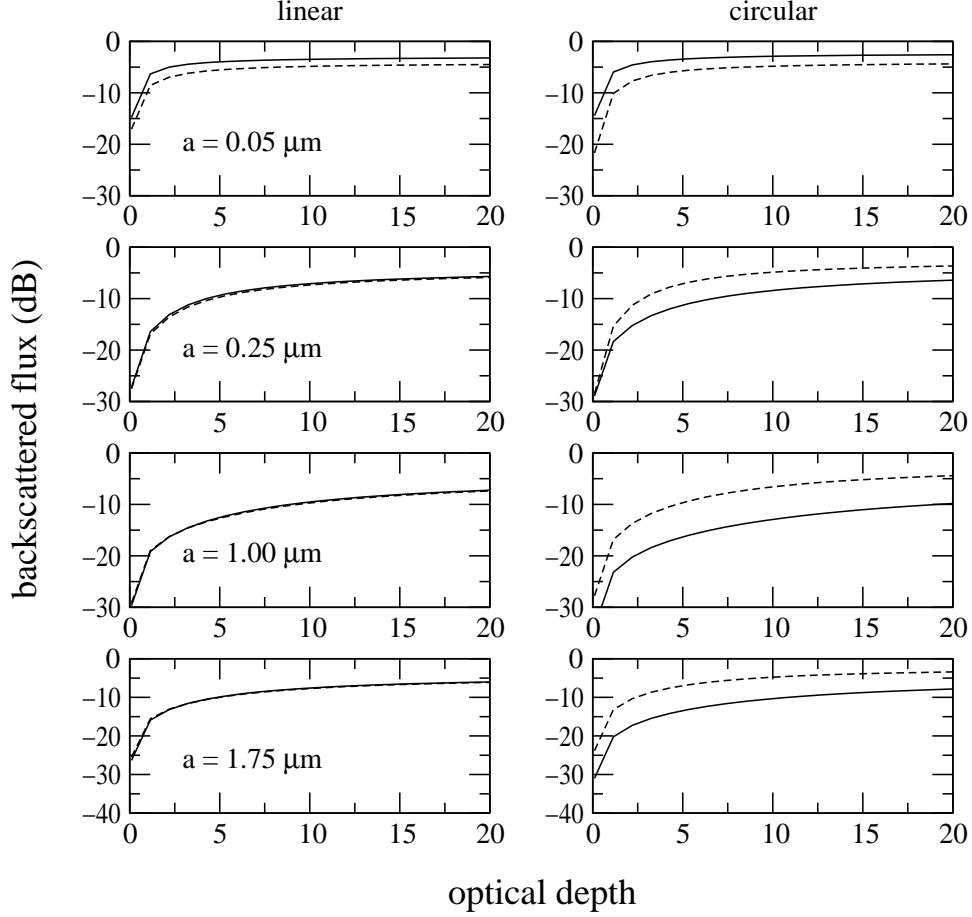


**Figure 3.** The diffuse backscattered flux responses for the linearly polarized waves (left column) and circularly polarized waves (right column). The plots on the first row from the top correspond to  $0.05\mu\text{m}$  radius spheres; the second row corresponds to  $0.25\mu\text{m}$  radius spheres; the third row corresponds to  $1.00\mu\text{m}$  radius spheres; and the fourth row corresponds to  $1.75\mu\text{m}$  radius spheres. The solid lines correspond to the co-polarized flux and the dashed lines correspond to the cross-polarized flux.

**Table 2.** Co-polarized and cross-polarized transmitted and backscattered flux differences at  $\tau_o = 20$  for linearly and circularly polarized incident waves.

radius ( $\mu\text{m}$ )	transmitted		backscattered	
	linear (dB)	circular (dB)	linear (dB)	circular (dB)
0.05	6.5E-5	1.3E-5	1.2734	1.7711
0.25	0.2827	2.0571	0.1838	2.7555
1.00	1.9315	7.4400	0.1495	5.4003
1.75	0.9142	4.1145	0.1062	4.4135

to the linearly polarized incident wave results, the flux responses by circularly polarized incident wave show larger flux differences as well as a stronger dependence on the size of the scatterers. This flux difference is largest for near-resonant scatterers in which there is a  $\sim 5$  dB difference between the co-polarized and cross-polarized flux.

Another qualitative difference between the linear and circular cases is that for circularly polarized incident waves, a polarization “flip” occurs in which the cross-polarized flux is larger than the co-polarized flux. To investigate this phenomenon in more detail, we examine the first order scattering solution. In Fig. 4, we plot the degree of

polarization

$$m_{\text{circular}} = \frac{I_{\text{co-pol}} - I_{\text{x-pol}}}{I_{\text{co-pol}} + I_{\text{x-pol}}} \quad (28)$$

computed from first-order scattering as a function of the cosine of the scattering angle. This figure shows the complicated angular dependence of the backscattered light. Furthermore, the values of the degree of polarization indicate changes in helicity from co-polarized ( $m_c > 0$ ) to cross-polarized ( $m_c < 0$ ). Since interpreting these angular spectra is not immediately intuitive, we computed the corresponding fluxes which appear in Table 3. From these flux computations, we observe that the three larger spheres show a helicity flip in which the cross-polarized flux is larger than the co-polarized flux. Hence, this polarization flip is present in first-order scattering and by observing the fluxes at larger optical depths, we see that this phenomenon becomes more pronounced.

#### 4. CONCLUSIONS

In this paper, we numerically solved the vector radiative transfer equation to examine basic polarization phenomena as well as the differences manifested from linearly and circularly polarized incident waves. Through our numerical investigations of backscattering and transmission through a plane-parallel medium containing monodisperse spherical scatterers, we found that circularly polarized incident waves maintain larger differences between co-polarized and cross-polarized fluxes and stronger dependencies on the sphere size, even at large optical depths (except for nearly Rayleigh scattering), than linearly polarized incident waves. These differences are most pronounced for scatterers that lie within or near the Mie resonance regime.

Except for scatterers in the Rayleigh limit, we found that transmitted circularly polarized incident waves depolarize at a slower rate than linearly polarized ones. For larger spheres, we find that this difference is significant. In particular, for near-resonance scatterers, circularly polarized waves exhibit co/cross-polarized flux differences of approximately 7 dB while linearly polarized waves exhibit approximately 2 dB flux differences. In addition to depolarizing slower than linearly polarized waves, circularly polarized waves exhibit a stronger dependence on the size of the scatterers. In experimental studies of tissue samples, differences between circular and linear polarized light are not nearly as significant as those observed for spherical scatterers.<sup>11,12</sup> Furthermore, linear polarized light maintains a larger degree of polarization than circular polarized light in tissues. Since tissues exhibit markedly different polarization characteristics than phantoms made up of spherical scatterers, some more effort should be given to understanding the polarization characteristics of tissues.

**Table 3.** Fluxes of backscattered circularly polarized light by an optically thin medium ( $\tau_o = 0.01$ ) of spherical scatterers computed using the first-order scattering solution.

radius ( $\mu m$ )	co-polarized flux (dB)	cross-polarized flux (dB)
0.05	-24.2310	-32.4692
0.25	-38.9421	-38.8451
1.00	-43.9701	-37.9167
1.75	-41.1327	-33.9478

In addition, we found that backscattering from circularly polarized incident waves exhibited a large degree of polarization for all of the scatterers that we have examined. For the  $0.05\mu m$  and  $0.25\mu m$  radii spherical scatterers, the co-polarized and cross-polarized flux difference is approximately 2 – 3 dB at large optical depths. For the  $1.00\mu m$  radius spherical scatterer, we find the largest difference between co-polarized and cross-polarized fluxes at approximately 5.4 dB over all optical depths that we considered. The  $1.25\mu m$  radius spherical scatterer case yields an approximate flux difference of 4.4 dB at large optical depths. We observe that the helicity of circular polarized light flips upon backscattering by the three larger spheres. While this characteristic is present in first-order scattering, it becomes slightly more pronounced as the optical thickness increases. Theoretical descriptions of this helicity flip usually include multiple scattering arguments,<sup>15,17</sup> however, a detailed analysis of first-order scattering may reveal a more basic mechanism for this helicity flip.

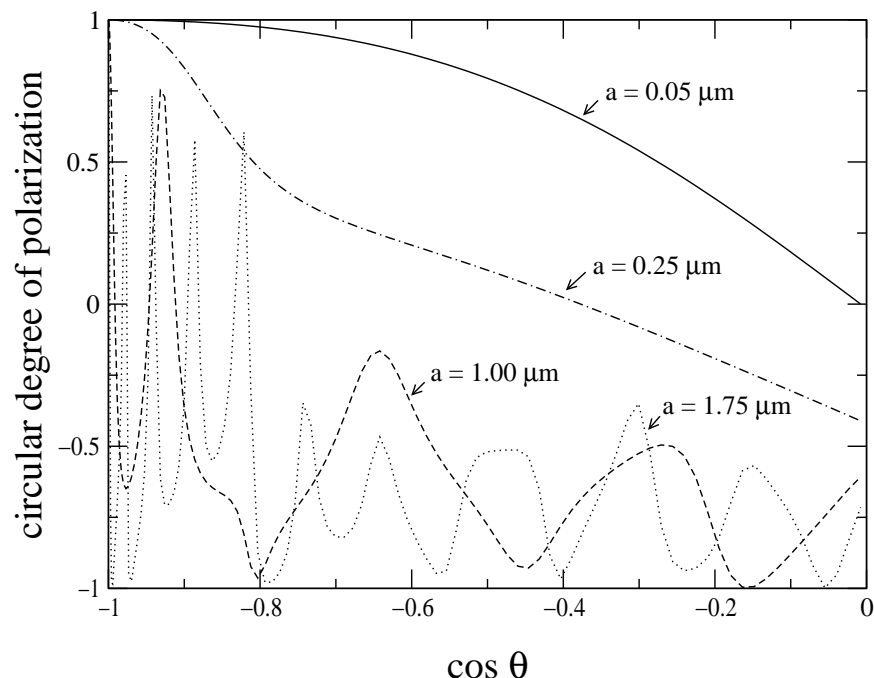


**Figure 4.** The degree of polarization for circular polarized light backscattered by an optically thin ( $\tau_o = 0.01$ ) slab containing spherical scatterers computed using the first-order scattering solution.

#### ACKNOWLEDGMENTS

This research was also supported by the National Science Foundation, the Office of Naval Research, the Air Force Research Laboratory and the Army Research Office. Arnold D. Kim would also like to acknowledge his support from the National Science Foundation (DMS-0071578).

#### REFERENCES

1. S. Chandrasekhar, *Radiative Transfer*, Dover, New York, 1960.
2. A. Ishimaru, *Wave Propagation and Scattering in Random Media*, IEEE Press, New York, 1997.
3. A. H. Hielscher, J. R. Mourant, and I. J. Bigio, "Influence of particle size and concentration on the diffuse backscattering of polarized light from tissue phantoms and biological cell suspensions," *Appl. Opt.* **36**, pp. 125–135, 1997.
4. S. G. Demos and R. R. Alfano, "Optical polarization imaging," *Appl. Opt.* **36**, pp. 150–155, 1997.
5. K. M. Yoo and R. R. Alfano, "Time resolved depolarization of multiple backscattered light from random media," *Phys. Lett. A* **142**, pp. 531–536, 1989.
6. J. M. Schmitt, A. H. Gandjbakhche, and R. F. Bonner, "Use of polarized light to discriminate short-path photons in a multiply scattering medium," *Appl. Opt.* **31**, pp. 6535–6546, 1992.
7. S. L. Jacques, J. R. Roman, and K. Lee, "Imaging superficial tissues with polarized light," *Lasers in Surgery and Medicine* **26**, pp. 119–129, 2000.
8. M. Moscoso, J. B. Keller, and G. C. Papanicolaou, "Depolarization and blurring of optical images by biological tissues." to be published in *J. Opt. Soc. Am. A*.
9. E. E. Gorodnichev, A. I. Kuzoviev, and D. B. Gogozkin, "Diffusion of circularly polarized light in a disordered medium with large-scale inhomogeneities," *JETP Lett.* **68**, pp. 22–28, 1998.
10. D. Bicout, C. Brosseau, A. S. Martinez, and J. M. Schmitt, "Depolarization of multiply scattered waves by spherical diffusers: Influence of the size parameter," *Phys. Rev. E* **49**, pp. 1767–1770, 1994.
11. V. Sankaran, M. J. Everett, D. J. Maitland, and J. T. W. Jr., "Comparison of polarized-light propagation in biological tissue and phantoms," *Opt. Lett.* **24**, pp. 1044–1046, 1999.

12. V. Sankaran, J. T. W. J. K. Schönenberger, and D. J. Maitland, "Polarization discrimination of coherently propagating light in turbid media," *Appl. Opt.* **38**, pp. 4252–4261, 1999.
13. E. E. Gorodnichev, A. I. Kuzoviev, and D. B. Gogozkin, "Depolarization of light in small-angle multiple scattering random media," *Laser Physics* **9**, pp. 1210–1227, 1999.
14. E. E. Gorodnichev, A. I. Kuzoviev, and D. B. Gogozkin, "Propagation of circularly polarized light in media with large-scale inhomogeneities," *J. Experim. and Theoret. Phys.* **68**, pp. 22–28, 1998.
15. F. C. MacKintosh, J. X. Zhi, D. J. Pine, and D. A. Weitz, "Polarization memory of multiply scattered light," *Phys. Rev. B* **40**, pp. 9342–9345, 1989.
16. K. J. Peters, "Coherent-backscatter effect: A vector formulation accounting for polarization and absorption effects and small or large scatterers," *Phys. Rev. B* **46**, pp. 801–812, 1992.
17. G. D. Lewis, D. L. Jordan, and P. J. Roberts, "Backscattering target detection in a turbid medium by polarization discrimination," *Appl. Opt.* **38**, pp. 3937–3944, 1999.
18. A. D. Kim and A. Ishimaru, "A Chebyshev spectral method for radiative transfer equations applied to electromagnetic wave propagation and scattering in a discrete random medium," *J. Comput. Phys.* **152**, pp. 264–280, 1999.
19. A. Ishimaru and R. L.-T. Cheung, "Multiple scattering effects on wave propagation due to rain," *Ann. Télécommunic.* **35**, pp. 373–379, 1980.
20. R. L.-T. Cheung and A. Ishimaru, "Transmission, backscattering, and depolarization of waves in randomly distributed spherical particles," *Appl. Opt.* **21**, pp. 3792–3798, 1982.
21. A. Ishimaru, *Electromagnetic Wave Propagation, Radiation and Scattering*, Prentice-Hall, Englewood Cliffs, New Jersey, 1991.
22. M. Kerker, *The Scattering of Light and Other Electromagnetic Radiation*, Academic Press, New York, 1969.
23. H. C. van de Hulst, *Light Scattering by Small Particles*, Dover, New York, 1981.
24. C. F. Bohren and D. R. Huffman, *Absorption and Scattering of Light by Small Particles*, John Wiley & Sons, New York, 1983.